JGR Space Physics

RESEARCH ARTICLE
10.1029/2024JA032547

Distinguishing Density and Wind Perturbations in the Equatorial Thermosphere Anomaly

A. Buynovskiy[1], J. P. Thayer[1,2], and E. K. Sutton[2]

[1]Aerospace Engineering Sciences Department, University of Colorado Boulder, Boulder, CO, USA, [2]Space Weather Technology, Research, and Education Center, University of Colorado Boulder, Boulder, CO, USA

Key Points:

- Accelerometer observations of the Equatorial Thermosphere Anomaly (ETA) cannot distinguish between in-track density and wind perturbations
- A new technique is applied to observations determining that the ETA, occurring between 9 and 16 LT, is a density-dominated feature
- The ETA demonstrates repeatable annual behavior for each season, suggesting a common and persistent formation mechanism

Correspondence to:

A. Buynovskiy,
Anton.Buynovskiy@colorado.edu

Citation:

Buynovskiy, A., Thayer, J. P., & Sutton, E. K. (2024). Distinguishing density and wind perturbations in the equatorial thermosphere anomaly. *Journal of Geophysical Research: Space Physics*, *129*, e2024JA032547. https://doi.org/10.1029/2024JA032547

Received 13 FEB 2024
Accepted 21 MAY 2024

Abstract In this paper, the equatorial thermosphere anomaly (ETA) is investigated using accelerometer measurements to determine whether the feature is density-dominated, wind-dominated, or some combination of the two. An ascending-descending accelerometry (ADA) technique is introduced to address the density-wind ambiguity that appears when interpreting the ETA in atmospheric drag acceleration analyses. This technique separates ascending and descending acceleration measurements to determine if a wind's directionality influences the interpretation of the observed ETA feature. The ADA technique is applied to accelerometer measurements taken from the Challenging Minisatellite Payload mission and has revealed that the ETA is primarily density-dominated from 9:00 to 16:00 local time (LT) near 400 km altitude, with the acceleration perturbations behaving similarly between 2003 and 2004 across all seasons. This finding suggests that the perturbations in the acceleration due to in-track wind perturbations are small compared to the perturbations due to mass density, while indicating that the formation mechanisms across these local times are similar and persistent. The results also revealed that in the terminator region at 18:00 LT the acceleration perturbations deviate appreciably between ascending and descending passes, indicating different or multiple processes occurring at this local time compared to the 9:00–16:00 LT ascribed to the ETA. These results help constrain ETA formation theories to specific local times and thermospheric property responses without the use of supplemental wind measurements, while also indicating regions where in-track winds cannot always be neglected.

Plain Language Summary Earth's thermosphere, a layer in the upper atmosphere, is a highly variable region that contributes to satellite drag in low Earth orbit. The equatorial thermosphere anomaly (ETA) is a perturbation feature that produces increases and decreases in drag accelerations across the lower latitudes of the thermosphere. Direct measurements of the thermosphere are often limited, so satellite instruments, such as accelerometers, have been used to analyze the acceleration that a satellite experiences due to atmospheric drag to indirectly measure thermospheric properties. However, the measured drag acceleration is dependent on both mass density and wind, making it difficult to determine whether a change in drag across the ETA is due to either property. This has implications on what mechanisms are responsible for its formation. This work introduces an ascending-descending accelerometry technique to exploit the fact that while acceleration perturbations produced by mass density are independent of satellite direction, those arising from winds can either be positive or negative depending on the relative spacecraft motion. By separating satellite orbits into ascending (south-to-north) and descending (north-to-south) passes, it can be determined whether drag acceleration perturbations are due to mass density, wind, or a mixture of the two, helping constrain possible formation mechanisms.

1. Introduction

Earth's thermosphere is a highly dynamic and coupled domain due to its interactions with the ionosphere and is susceptible to energy and momentum transfer from the sun, magnetosphere, and lower atmosphere. With such a complex domain comes a multitude of dynamic and thermodynamic neutral gas processes, many of which are not fully understood. Better comprehension of these mechanisms will aid in low Earth orbit (LEO) environmental conditions forecasting, satellite operations, precise orbit determination (POD) and prediction, and radio communication protocols. This incomplete understanding of the thermosphere can be traced to the limited coincident measurements of mass density, winds, temperature, and composition. In the 1960 s through the 1980 s, the upper atmosphere was studied fervently, giving life to many in-situ measuring satellite missions, such as the Dynamics Explorer 2 (DE-2), Atmospheric Explorers (AE), Orbiting Geophysical Observatory 6 (OGO-6), Orbiting Vehicle 3–6 (OV3-6), European Space Research Organization 4, and Aeros A/B. Beyond the 1980 s,

efforts to take in-situ measurements of the thermosphere were abated and large-scale missions focusing on remote sensing measurements were pursued. Such missions include the Upper Atmosphere Research Satellite (UARS), the Thermosphere-Ionosphere-Mesosphere-Energetics and Dynamics (TIMED) mission, the Global-scale Observations of the Limb and Disk (GOLD) mission, and the Ionospheric Connection Explorer (ICON).

In the last 20 years, on-board accelerometry techniques have been utilized extensively for atmospheric drag analyses to improve POD methods and extract thermospheric properties such as mass density and cross-track winds (e.g., Bruinsma & Biancale, 2003; Doornbos et al., 2010; Sutton et al., 2007). These science-grade accelerometry techniques have been used with missions such as the Challenging Minisatellite Payload (CHAMP) (Reigber et al., 2002), Gravity Recovery and Climate Experiment (GRACE) (Tapley et al., 2004), GRACE-FO (Kornfeld et al., 2019), Gravity Field and Stead-State Ocean Circulation Explorer (GOCE) (Floberghagen et al., 2011), and Swarm (Olsen et al., 2013). There have also been ground-based remote sensing instruments trained on the thermosphere for many years, such as the Fabry-Perot Interferometer and all-sky imagers, as well as rocket campaigns which measured various in-situ properties of the thermosphere. Much of the thermospheric data collected from past observations have been integrated into empirical models, such as the Horizontal Wind Model (HWM) (Drob et al., 2015) and the Mass Spectrometer Incoherent Scatter (MSIS) model (Emmert et al., 2020), to offer a climatological understanding of thermospheric properties. Physics-based models, such as the Thermosphere-Ionosphere-Electrodynamics General Circulation Model (TIEGCM), have also been instrumental in understanding what variables contribute to thermospheric mechanisms using fundamental momentum, energy, and mass continuity equations (Qian et al., 2014). All these efforts have been vital in characterizing the thermosphere, yet there are still knowledge gaps as more datasets reveal discrepancies with models (Bruinsma et al., 2022; Dhadly et al., 2023).

One thermospheric feature whose structure, formation, and evolution processes are still in question is the equatorial thermosphere anomaly (ETA). The ETA has been described in a multi-property manner since its initial observations. It was first introduced as having a distinct N_2 and O_2 density minimum located near the magnetic equator (Hedin & Mayr, 1973; Philbrick & McIsaac, 1972). These measurements were obtained from the neutral mass spectrometers on OGO-6 between 400 and 500 km at 17:00 LT near the autumnal equinox, as well as from OV3-6 near 400 km at local sunset. Later, Raghavarao et al. (1991) discussed a correlation among zonal winds, neutral temperature, and the Equatorial Ionization Anomaly (EIA), labeling this phenomenon the Equatorial Temperature and Wind Anomaly (ETWA). These measurements were obtained from the Wind and Temperature Spectrometer (WATS) on the DE-2 satellite between 280 and 600 km altitude near 11:00 and 19:00 LT during spring and autumn. Not long after, Raghavarao et al. (1993) discussed how vertical winds might also be related to the ETWA description. This observation was also made by the WATS instrument on the DE-2 mission between 300 and 430 km altitude at 21:00 LT in the spring. Liu et al. (2005) was the first to reveal a persistent equatorial mass density structure in the thermosphere and associated it with the EIA structure from concurrent ionospheric measurements. The mass density measurements were indirectly derived from the Spatial Tri-axial Accelerometer for Research (STAR) onboard CHAMP around 400 km across all local times in 2002. The mass density structure was later labeled as the equatorial mass density anomaly (EMA) from a climatological study (see Liu et al., 2007), where a mass density minimum near the dip equator with two maxima on both sides was linked to the EIA. These density measurements were also indirectly derived from STAR onboard CHAMP around 400 km at 11:00–16:00 LT over a four year period. Lei et al. (2010) generalized the description as the equatorial thermosphere anomaly, using past observations of the thermosphere and ionosphere, as well as CHAMP accelerometry to characterize the ETA properties more accurately. Finally, Clemmons et al. (2013) suggested there are strong, magnetically aligned alternating meridional winds, up to 700 m/s, associated with the ETA description. These wind measurements were indirectly derived using the ionization-gauge from the Streak mission between 275 and 325 km altitude and confined to the dusk sector over a 10 month period.

CHAMP accelerometry has been extremely valuable in describing the ETA, as it has provided the largest database of ETA observations to date with a decade's worth of highly sensitive accelerometer data. The recorded accelerations have an inherent dependence on thermospheric mass density and winds that is often not fully separable by a single measurement. This is particularly true for accelerations experienced in the direction of the satellite track where mass density and in-track thermospheric winds can both contribute to the measured accelerations. Accelerometers are more sensitive to the range of mass density changes than they are to the range of winds in the thermosphere because winds are typically a small part of the total inertial velocity experienced by the satellite. This often leads to the assumption that in-track accelerations are primarily due to mass density changes (e.g.,

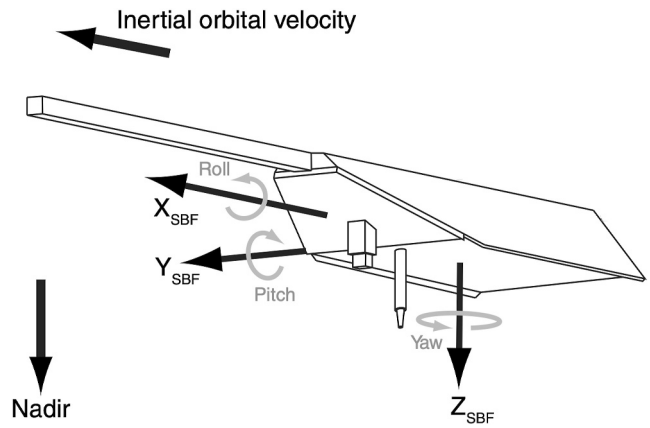

Figure 1. CHAMP SBF axes with X_{SBF} in the velocity vector (in-track), Y_{SBF} in the cross-track direction, and Z_{SBF} in the nadir direction (Adapted from Doornbos et al., 2010).

Bruinsma & Biancale, 2003; Liu et al., 2006; Sutton et al., 2007). However, thermospheric winds in the track of a LEO satellite can reach sufficient magnitudes to cause detectable acceleration perturbations and affect the interpretation of accelerometer measurements. The purpose of this study is to investigate whether the ETA, as observed by in-track acceleration perturbations in the CHAMP satellite accelerometer, is a density-dominated perturbation, wind-dominated perturbation, or a combination of the two. By employing a novel accelerometry approach, the influence of wind magnitude and directionality on in-track accelerations can be evaluated to better describe the ETA perturbation and help expose potential processes occurring in the thermosphere responsible for its formation.

2. Approach

2.1. Accelerometry

The general principle behind accelerometry is to characterize the forces imposed on the body that contribute to a net acceleration. For an orbiting satellite, accelerometry can be used to measure non-gravitational acceleration perturbations due to drag, lift, and radiation pressure (Bruinsma & Biancale, 2003; Doornbos et al., 2010; Sutton et al., 2007). On-board accelerometry techniques have been used extensively for atmospheric drag analyses to extract thermospheric properties such as mass density and cross-track winds, which have achieved reasonable success (Doornbos et al., 2010; Siemes et al., 2023). However, these extraction methods require knowledge of the in-track winds, which have been addressed by either neglecting the in-track winds or modeling the in-track winds using HWM and absorbing the wind effect as a contributing error to the density/cross-track wind estimates (e.g., Bruinsma & Biancale, 2003; Bruinsma et al., 2022; Doornbos et al., 2010; Sutton et al., 2007). Even with these solutions, one of the largest uncertainties for mass density and cross-track wind derivations comes from the uncertainties in the in-track wind, limiting the interpretation of these derivations.

This investigation focuses on in-track accelerometer data from the CHAMP mission, which operated from 2000 to 2010 at an inclination of 87.3° and an initial altitude of 454 km, to infer in-track wind behavior. Onboard CHAMP was a highly sensitive accelerometer called STAR, which captured 10 years' worth of continuous acceleration data at a cadence of 10 s and a precision of 3×10^{-9} m/s^2 in the high-sensitivity axes (Reigber et al., 2003). STAR was situated at CHAMP's center of mass so that the reference frame of the instrument is aligned with the satellite body fixed (SBF) frame as shown in Figure 1.

CHAMP also had an attitude control error of ±0.01°, as well as POD solutions from the GPS system and the laser ranging network (Reigber et al., 2003), making it a valuable tool for drag acceleration analyses. Using knowledge of CHAMP's position, velocity, orientation, structural properties, and accelerometer data, the secondary non-conservative forces (solar radiation pressure, Earth's albedo, and Earth's infrared radiation) acting on the spacecraft can be modeled and isolated from atmospheric drag (e.g., Bruinsma & Biancale, 2003; Doornbos et al., 2010; Siemes et al., 2023; Sutton et al., 2007). This procedure allows for a direct relationship between the drag acceleration and the STAR data using the following equation:

$$\boldsymbol{a}_d = -\frac{\rho}{2m} C_d A |\boldsymbol{v}| \boldsymbol{v} \tag{1}$$

Equation 1 shows how the drag acceleration variables (with bold font to indicate vectors) are related to the accelerometer data, where $\boldsymbol{a}_d$ is the retrieved drag acceleration, $\mathbf{C}_\mathrm{d}$ is the coefficient of drag, A is the reference area, m is the spacecraft mass, ρ is the thermospheric mass density $\boldsymbol{v} = \boldsymbol{v}_{sc} - \boldsymbol{v}_{corot} - \boldsymbol{v}_{wind}$ is the relative velocity of the atmosphere with respect to the satellite, $\boldsymbol{v}_{sc}$ is spacecraft velocity, $\boldsymbol{v}_{corot}$ is the motion of an atmosphere co-rotating with the Earth, and $\boldsymbol{v}_{wind}$ is the thermospheric wind. The expression for the co-rotating atmospheric motion is $\boldsymbol{v}_{corot} = \boldsymbol{\omega} \times \boldsymbol{r}$, where ω is the Earth's angular velocity and r is the inertial satellite position. There are uncertainties associated with the modeling of the non-conservative forces as well as with the instrument capabilities, which will be addressed in Section 3.2.

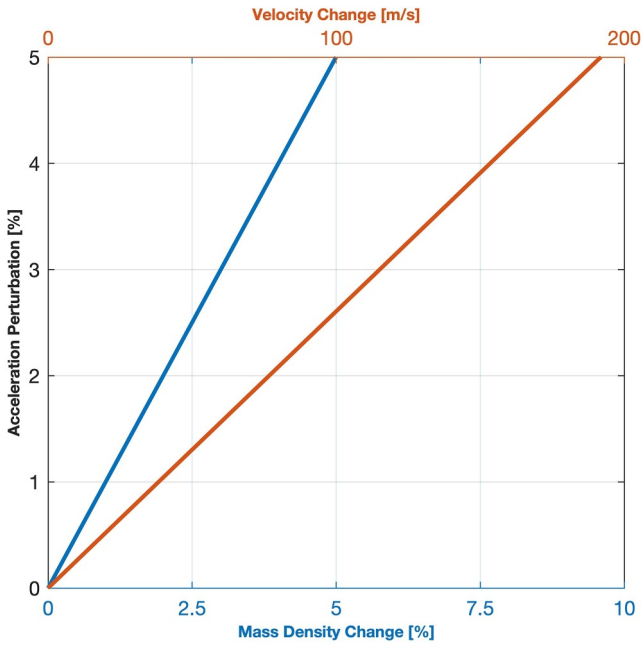

Figure 2. Acceleration perturbations caused by either a mass density or velocity change.

2.2. Density-Wind Ambiguity

When deriving thermospheric properties using drag accelerometry techniques, there are typically two thermospheric unknowns for a single measurement: mass density and wind. Without knowledge or assumptions on the mass density or wind structure, it is difficult to distinguish whether a change in the acceleration is associated with a density or wind perturbation. In the context of the CHAMP mission, it is the X_{SBF} axis that is most influenced by mass density and in-track winds.

To better quantify how the density-wind ambiguity arises in drag acceleration analyses, a perturbation analysis for the in-track component of Equation 1 is conducted to reveal the effects of mass density and wind perturbations on the acceleration. The percent change in acceleration due to a density perturbation is shown in Equation 2, where δa_ρ is the in-track acceleration perturbation due to a change in mass density, $\Delta\rho$ is the change in mass density, and ρ_o is the baseline mass density. The percent change in acceleration due to a velocity perturbation is shown in Equation 3, where δa_w is the in-track acceleration perturbation due to a change in wind, Δv_{wind} is the change in the in-track wind, and $v_{0,x} = v_{sc,x} - v_{corot,x} - v_{wind,x}$. For this scenario, $v_{sc,x} = 7.67$ km/s, $v_{corot,x}$ is negligible for the in-track direction for high-inclination satellites, and $v_{wind,x}$ is baselined at 0 m/s.

$$\delta a_\rho = \frac{\Delta\rho}{\rho_o} * 100 \tag{2}$$

$$\delta a_w = \frac{2\Delta v_{wind}}{v_{o,x}} * 100 \tag{3}$$

Figure 2 displays the sensitivity that the drag acceleration has to a change in the mass density or wind, revealing the level of wind perturbations and density changes required to generate the same acceleration changes. Mass density is directly proportional to the drag acceleration, which means that for a 5% change in the acceleration measurements, there needs to be a 5% change in the background mass density. A perturbation in the velocity can be attributed to a change in the thermospheric wind. Figure 2 illustrates that when a wind magnitude changes from being stagnant to almost 200 m/s, a 5% change in acceleration occurs. Both of these density and wind changes can occur in the thermosphere, so the density-wind ambiguity is a justifiable concern, especially when measurements for either property are limited.

This sensitivity analysis also reveals that while low-magnitude in-track winds produce little error when ignored in accelerometry analyses, this assumption can produce large errors when winds are large (an 800 m/s produces a>20% error), such as in the high-latitude regions (Lühr et al., 2007; Sutton et al., 2005). To improve the density and wind extraction methods using accelerometry, the work presented in this paper will directly characterize the in-track density and in-track wind perturbations without requiring supplemental wind measurements.

2.3. Ascending-Descending Accelerometry

With the desire to directly characterize the density and wind structures of the ETA without the need of additional wind measurements, this study developed an ascending-descending accelerometry (ADA) technique to overcome the inherent density-wind ambiguity. The basic principle of ADA is rooted in directionality: mass density is a scalar property, while winds are a vector property. The concept is that when a spacecraft ascends through a density-wind field, it can experience different accelerations than if it were to descend through the same density-wind field due to the wind's directionality. While a single orbit fly by grants one measurement for the two thermospheric unknowns, the ascending-descending technique unlocks additional information, making it more feasible to discern a density and wind perturbation.

For a single-satellite mission, a spacecraft cannot ascend and descend through a target region simultaneously to discern both in-track density and in-track wind; however, if the spacecraft were to precess such that the ascending

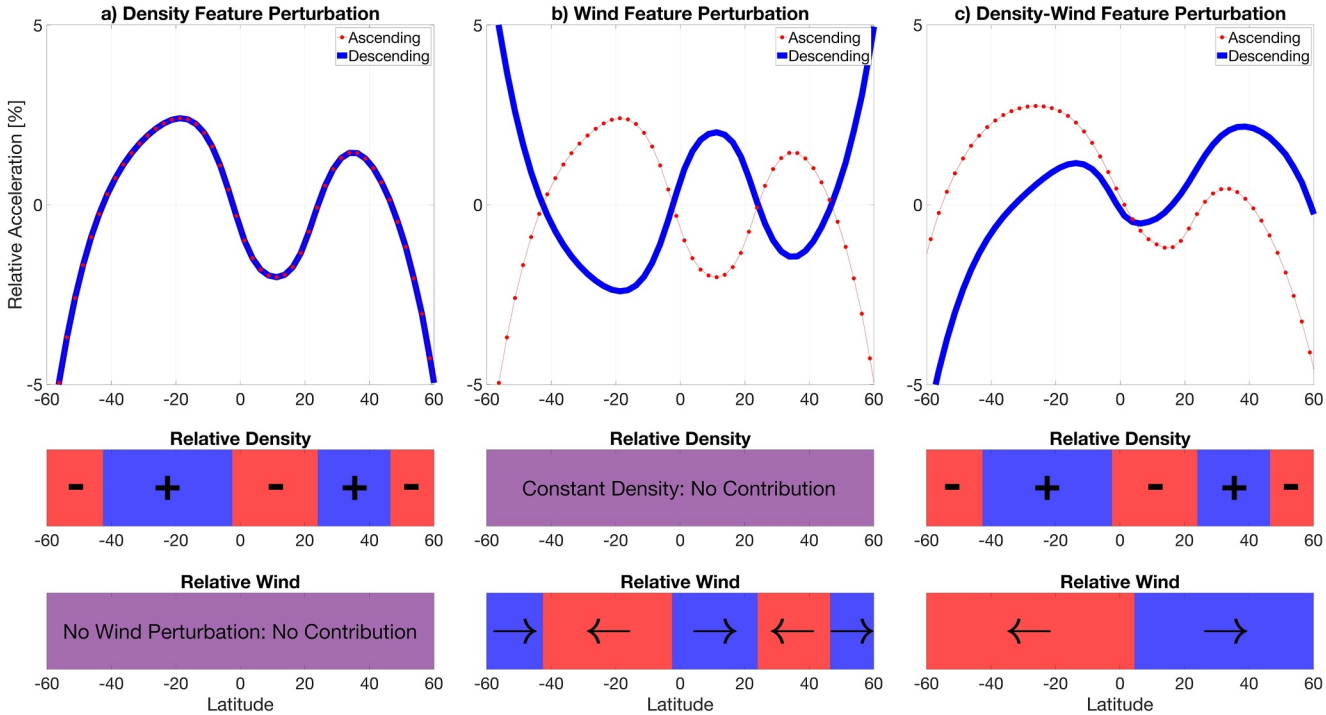

Figure 3. ADA relative acceleration (percent change) interpretations for (a) density feature perturbations, (b) wind feature perturbations, and (c) density-wind feature perturbations. The red shading represents a decrease in relative density/negative (southward) wind change, the blue shading represents an increase in relative density/positive (northward) wind change, and the purple shading represents a constant relative density/no wind perturbations that do not contribute to the relative acceleration.

and descending nodes are examining the same local time of a region, then under the right conditions, the ADA technique can be applied. The first condition for single-satellite ADA is that the satellite must ascend and descend through a target region with similar space environment conditions. Similar space environment conditions include, but are not limited to, similar local time, similar solar EUV flux levels in the solar cycle, similar geomagnetic conditions, similar time of year (season), and similar altitude. A second condition is that the satellite orbit be near-polar to mitigate in-track contributions from large co-rotating atmospheric motion and zonal winds, essentially being most sensitive to the in-track (meridional) winds. The third condition is that the target region must be focused on a persistent, recurring thermospheric phenomenon to ensure that the density and wind structures are recurring and not associated with transients or instabilities.

ADA is centered around analyzing how changes in density and wind fields affect relative acceleration measurements, with knowledge of the sensitivity of acceleration due to density and wind. Once the conditions for the single-satellite ADA are met, there are a few ways to interpret the outcomes. Figure 3 demonstrates three different interpretations of representative relative acceleration curves surrounding the ETA along with bars depicting the underlying relative density and wind structures that produced the resultant acceleration. The relative acceleration curves were modeled using thermospheric mass density and wind outputs from TIEGCM simulations to serve as a reference. It is important to note that Figure 3 describes fluctuations in the acceleration once background accelerations are removed. ADA is not a technique to characterize the total response of the density-wind structures, but a technique to determine whether a perturbed acceleration is due to a thermospheric perturbation that is density-dominated, wind-dominated, or a mixture of the two.

A density-dominated feature is one where perturbations in the acceleration are associated with a density perturbation much greater than those produced by a wind perturbation, meaning the wind perturbations can be considered insufficient to induce such an acceleration response. The elimination of winds from Equation 1 removes the unknown directional variable, leaving the acceleration perturbation to be a function of a scalar property, that is, mass density. This means that whether a satellite ascends or descends through a feature, the perturbation accelerations that the satellite experiences are the same. Figure 3a depicts how the relative accelerations match in the ascending and descending directions using thermospheric mass density outputs from

TIEGCM and assuming there is zero wind perturbation. This representative relative acceleration curve is characteristic of ETA accelerations presented in past literature (e.g., Lei et al., 2010; Liu et al., 2007).

A wind-dominated feature is one where changes in the acceleration due to a wind perturbation are much larger than those due to a density perturbation, allowing the density to be interpreted as constant. Treating the density as constant means that the only changing variable in Equation 1 is due to the directional wind. Figure 3b shows how the relative acceleration from Figure 3a responds to a constant density structure with a fictitious wind perturbation structure that alternates in direction. When a satellite ascends a region from −60° to 60° latitude as depicted in Figure 3b, it first experiences a negative relative acceleration because the positive (northward) wind is in the same direction as the satellite velocity vector, causing reduced drag. Then, the satellite experiences a positive relative acceleration as it orbits through a negative (southward) wind field because the wind direction is now opposite to the satellite velocity vector, yielding higher drag. Following this logic for the rest of the orbit path results in the depicted ascending relative acceleration curve, shown in red in Figure 3b. Conversely, when the satellite descends the region from 60° to −60° latitude assuming the same perturbation wind structure, it first experiences a positive relative acceleration because the satellite velocity vector is now opposite to the positive (northward) wind, yielding higher drag. The satellite then experiences a negative relative acceleration as it traverses a negative (southward) wind field, which is now in the same direction as the satellite velocity vector, causing reduced drag. Following this logic for the rest of the orbit path yields the depicted descending relative acceleration curve, shown in blue for Figure 3b. Here, the ascending relative acceleration curve is the same as the one shown in Figure 3a, demonstrating how the density-wind ambiguity comes into play, yet the descending orbit in Figure 3b reveals an inverse behavior while describing the same density and wind fields, highlighting the importance of directionality in ADA. This inverse behavior is characteristic of a wind-dominated feature.

A third conclusion is when both mass density and wind changes cause appreciable relative accelerations, as shown in Figure 3c. Here, the density structure is the same as the representative ETA density structure shown in Figure 3a but there is now an additional diverging wind field using an amplified wind structure (up to 200 m/s) from TIEGCM outputs. While the wind magnitudes are modified to emphasize the impact of wind perturbations on acceleration, the structure may be representative of the meridional wind structure in the thermosphere (Drob et al., 2015). When a satellite ascends through the region from −60° to 60° latitude, the relative accelerations reflect similar behaviors as shown in Figure 3a, but because it is also traversing a negative (southward) wind field, which is against the satellite velocity vector, the relative accelerations are increased. Then, as the satellite enters a positive (northward) wind field, which is now in the same satellite velocity direction, it also experiences relative accelerations similar to those in Figure 3a, but with decreased relative accelerations. As the satellite descends through the same region from 60° to −60° latitude, it first experiences relative accelerations that reflect similar behaviors as shown in Figure 3a, but because the positive (northward) wind is now in the opposite direction to the satellite velocity vector, the relative accelerations are decreased. Then as the satellite enters a negative (southward) wind field, the relative accelerations follow the similar behavior shown in Figure 3a., but with reduced drag since the wind is now in the same direction as the satellite velocity vector. This example shows how a density field modulated with a diverging wind field can skew, but not invert, relative acceleration plots between ascending and descending orbits.

For this paper, the ADA technique is applied to the CHAMP accelerometer data, as it fits the criteria specified. The eccentricity, inclination, and altitude of CHAMP cause the local time of the ascending node (LTAN) of the orbit to precess at an approximate rate of 12 hr every 131 days. In three precession periods, one year will have elapsed with about a 28 day advancement in season. At the same time, the local time previously sampled by the ascending (descending) node will now be sampled by the descending (ascending) node. Fortuitously, the orbit configuration of CHAMP meets ADA requirements one and two: the solar cycle period is similar (one year apart), the seasons are similar (28 days apart), the local time is the same, the altitudes are similar (~20 km difference, or about 1/3 of a scale height–with both normalized to the same altitude for analysis), and the orbit is near-polar. To satisfy the final requirement, the target region under investigation is the persistent and recurring daytime ETA phenomenon.

3. Data Description

3.1. Data Processing

For this study, acceleration measurements from CHAMP's STAR accelerometer from 2003 to 2004 are used. The acceleration measurements are the version 2.3 release of the CHAMP accelerometer-derived atmospheric densities provided by Sutton (2009). The dataset consists of raw accelerometer data at a cadence of 10 s in each of the STAR's three axes, CHAMP's orbit-ephemeris data, quasi-dipole magnetic coordinates, and the modeled accelerations due to solar radiation pressure, Earth's albedo radiation pressure, and Earth's infrared radiation pressure. With the focus of ADA being the in-track mass density and in-track winds, only the accelerometer data associated with the X_{SBF} direction is utilized. First, the modeled radiation pressures are removed from the non-conservative accelerometer data, leaving just the acceleration due to drag. Then, as is typically done with density measurements taken from CHAMP (e.g., Bruinsma & Biancale, 2003; Doornbos et al., 2010; Siemes et al., 2023; Sutton et al., 2007; Thayer et al., 2008), the in-track accelerations are normalized to a constant altitude of 400 km. However, while past literature normalized density to a constant altitude, this work concentrates on the acceleration. In order to extend past normalization procedures to the measured accelerations, the following steps are taken based on the drag acceleration from Equation 1, where $a_{400,x}$ and $\rho_{400,x}$ are the acceleration and mass density normalized to 400 km, $a_{o,x}$ and $\rho_{o,x}$ are the acceleration and mass density at the satellite altitude, $v_x = v_{sc,x} - v_{corot,x} - v_{wind,x}$, h_o is the satellite altitude in kilometers, and H is the scale height at the satellite altitude in kilometers.

$$\rho_{400,x} = \rho_{o,x} e^{\frac{h_o - 400}{H}}$$

$$\frac{2m}{v_x^2 C_d A} a_{400,x} = \frac{2m}{v_x^2 C_d A} a_{o,x} e^{\frac{h_o - 400}{H}}$$

$$a_{400,x} \approx a_{o,x} e^{\frac{h_o - 400}{H}} \tag{4}$$

This normalization assumes that the reference area, coefficient of drag, and satellite mass are constant between satellite and normalization altitudes. For the velocity term, changes in the satellite velocity and co-rotating atmospheric motion to the normalized altitude were evaluated and produced minimal effect over the range of satellite altitudes observed in this study. At the same time, the in-track winds are assumed to be constant with altitude due to the high molecular viscosity that minimizes vertical gradients in the wind velocity at this altitude (Richmond, 1983). The scale height is determined using the Naval Research Laboratory MSIS Extended model (NRLMSISE-00) for the mean molecular weight and neutral temperature (Picone et al., 2002).

$$a_{rel} = \left(\frac{a_{400,x}}{a_{filt}} - 1 \right) * 100 \tag{5}$$

To observe the relative accelerations surrounding the ETA, the normalized accelerometer data is filtered using a 99-data point moving average filter, which corresponds to 990 s, or a scale length of about 7,600 km. This low pass filtered data represents the large-scale background accelerations associated with large-scale thermospheric mass density and wind structures due, for example, to solar flux variations and variability introduced by migrating and non-migrating tides. The background data also absorbs large-scale effects caused by any systematic behavior introduced by changes in spacecraft characteristics, see Section 3.2. The normalized in-track accelerations are divided by the background accelerations for each orbit to produce percent change residuals that represent small- and medium-scale changes in acceleration. This filtering procedure is summarized in Equation 5, where $a_{400,x}$ is the acceleration and mass density normalized to 400 km and a_{filt} is the filtered acceleration representing the background. To also ensure that the ETA is in a stable condition and not influenced by geomagnetic variability, as shown in earlier studies (Lei et al., 2010), data points at times when the estimated 3-hr Kp index is greater than five are removed for this analysis. Figure 4 demonstrates the filtering process for a given dayside orbital pass. The residuals illustrate the ETA behavior in geomagnetic latitude, which has been well documented over the lifetime of the CHAMP mission (e.g., Lei et al., 2010; Liu et al., 2007).

Once the data is filtered and converted to a relative acceleration, it is then split into ascending and descending phases of the mission. In 2003, there were three distinct periods when CHAMP was measuring the local times associated with the ETA, the first and third occurred during descending passes while the second was during

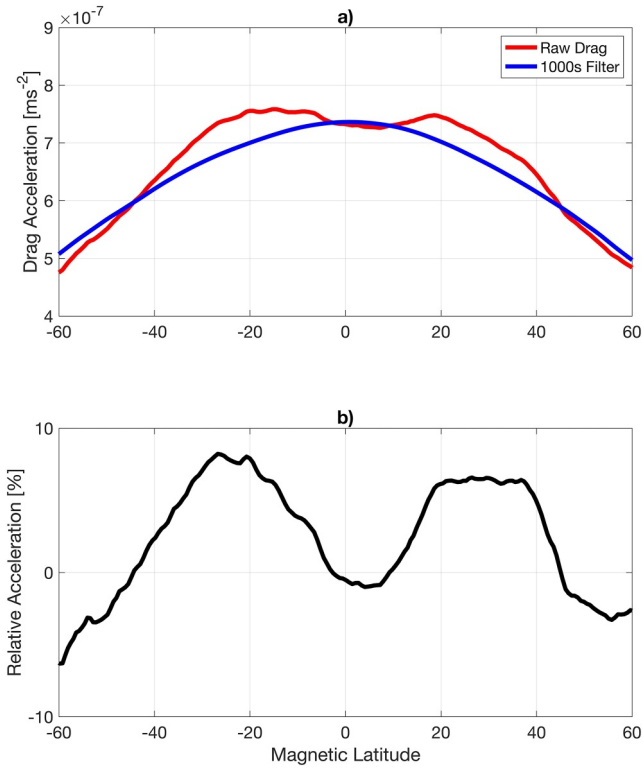

Figure 4. (a) Raw and 990 s filtered accelerometer measurements with respect to magnetic latitude taken at the equatorial dayside (15:00 LT) region for a single orbit on day 279 in 2003 and (b) relative acceleration per Equation 5.

ascending passes. Similarly, in 2004, there were three periods roughly corresponding to those in 2003, but with switched ascending/descending configuration. Once the data is split into the ascending and descending phases, they are binned and averaged into local time and latitude intervals. Since the ETA has been demonstrated to be magnetically controlled (Liu et al., 2005), the latitude bins are organized in magnetic latitude. The magnetic latitude bins range between ±60° and have intervals of 2° to capture small- and medium-scale structures in the residual accelerations. The local times are binned into 30 min intervals across the dayside. In a portion of an orbit between ±60° latitude, there will be a slight range in local time, which results in about eight days' worth of accelerometer data per 30 min LT bin, a few days larger than the LTAN precession rate.

3.2. Error Analysis

The CHAMP accelerometer data derived through the ADA procedure is subject to multiple sources of systematic and noise errors. The recognized systematic errors are related to the instrument calibration, spacecraft behavior, and environmental conditions. The systematic instrument errors are due to the bias and scale factors in STAR's calibration. The systematic errors related to the spacecraft behavior (i.e., attitude uncertainty) are considered negligible as CHAMP's attitude error of ±0.01° has a minimal effect on the variables contributing to drag (e.g., ρ, v, and the product C_dA). The radiation pressure model used to isolate the drag acceleration is also recognized as a source of systematic error. Over long time periods, error in the radiation pressure model resembles noise error, but because the ADA technique only focuses on a fraction of an orbit and the vehicle attitude does not change appreciably, this modeling can be viewed as a systematic error. There are also systematic errors associated with the discussed seasonal shift, trends in the solar flux, and long-term variability in the geomagnetic activity. All the non-negligible systematic errors are mitigated when the background acceleration is removed in the ADA procedure. The relevant noise errors are due to the STAR's instrument precision as well as the geophysical variance among various orbits. The in-track accelerometer axis (X_{SBF}) has a precision of 3×10^{-9} m/s^2 (Reigber et al., 2002), which when propagated, causes less than 0.1% uncertainty in the relative accelerations, rendering the instrument precision error negligible. The remaining noise errors are due to geophysical variability and can be attributed to measurements being taken at varying longitudes, universal times, seasons, and geomagnetic conditions in the 8 days' worth of accelerometer data captured in each local time profile. To quantify the data spread due to the geophysical variability, the standard error of the mean is calculated to assess the variability across multiple orbits of the residual accelerations.

4. Results

4.1. Resolving the ETA

For this ADA study, the filtering and binning procedures result in relative accelerations due to density-wind structures associated with the ETA. Figure 5 demonstrates the mean outcome for a descending orbit period (spanning days 55–63) in 2003 for 30 min of local time centered at 11:00 LT in a relative acceleration versus magnetic latitude plot. Here, the mean of the relative acceleration has been determined from approximately eight days' worth of continuous descending orbits with the width of the line quantifying the uncertainty of the mean - primarily due to geophysical noise accumulated over the days that contribute to the specific 30 min local time interval. Two crests can be recognized near ±20°–30°in magnetic latitude along with a trough near the magnetic equator, which are consistent with past accelerometer observations of the ETA (e.g., Lei et al., 2010; Liu et al., 2007).

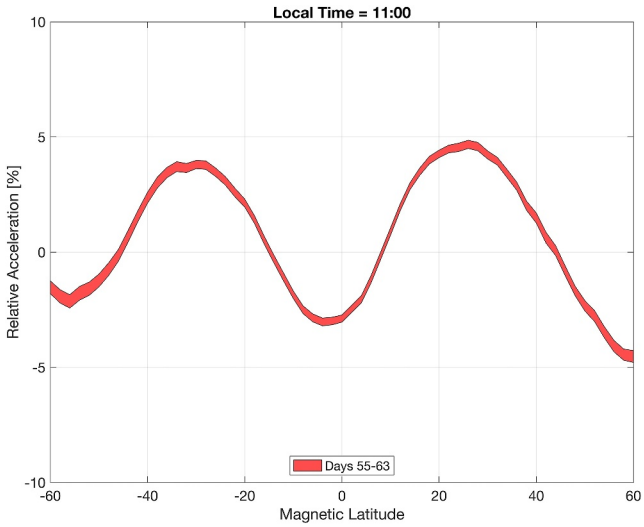

Figure 5. Descending relative acceleration (percent change) with respect to magnetic latitude in 2003 at 11:00 LT near the vernal equinox displaying the characteristic signature of the ETA. The width of the line quantifies the uncertainty of the mean.

4.2. Comparing the ETA Between 2003 and 2004

Figure 6 summarizes the ETA results from the ADA technique between 2003 and 2004. These results are organized into three different times of year and at three representative dayside local times to illustrate the behavior in the relative accelerations for ascending and descending orbits surrounding the ETA. In almost all the cases in Figure 6, and for cases not shown that lie between 9:00 and 16:00 LT, the ETA's crests and troughs can be detected in both the ascending and descending directions. For a general overview, there are recognized seasonal differences in the relative acceleration structures surrounding the ETA when observing the same local time, identified by Liu et al. (2007). Similarly, the relative acceleration structures vary somewhat with respect to the local time while observing a similar time of year. The relative changes in the ascending and descending directions for the same local time and season harmonize exceptionally well, with the thickness of the uncertainty bands averaging around 0.5% on the relative acceleration scale and an average difference between means of 1.2% for the ascending and descending directions.

5. Discussion

5.1. Thermospheric Observations

The ADA technique utilizes accelerometer datasets from single-satellite missions to help resolve the density-wind ambiguity that arises with drag acceleration analyses. Following the procedure for ADA using CHAMP accelerometry, the results from Section 4 revealed that the ascending and descending measurements are nearly harmonized, which indicates a density-dominated ETA feature according to Section 2.2. This interpretation is an important finding as it demonstrates in-track density changes are more influential on the accelerometry measurements surrounding the ETA than in-track (or roughly meridional) wind changes without the need for supplemental wind measurements or wind models. This inference also corroborates the assumption that winds are insufficient to produce the observed acceleration perturbation structure in the region surrounding the ETA, addressing the density-wind ambiguity in this region. The ADA analysis revealed that throughout various seasons, from 9:00 to 16:00 LT and near 400 km altitude, the ETA is primarily density-dominated with the relative accelerations behaving similarly between 2003 and 2004 regardless of orbit direction. This reinforces past findings that the mechanisms involved in forming the ETA are those that produce a mass density change across the equatorial region with a mass density trough over the magnetic equator flanked by two mass density crests (e.g., Hsu et al., 2014; Lei et al., 2012; Liu et al., 2005).

While this analysis has revealed that the ETA is primarily density-dominated, the ascending and descending perturbations are not always exactly co-registered, with differences such as minor phase shifts, varying crest magnitudes, and varying trough magnitudes. These variations could be due to changes in the density-wind perturbation field ascribed to (a) the difference in one year in the solar cycle, (b) seasonal differences due to the 28 day seasonal shift between years, and (c) varying geomagnetic conditions between years. To ensure that there are no local or systematic variations due to the filtering approach, an analysis of the removed background accelerations was carried out. This revealed that the ascending and descending background accelerations have very similar structures across the different seasons and local times, albeit of different magnitudes. The background accelerations absorb large-scale changes due to such effects as solar flux variations impacting mass density, prevailing wind fields, or even any large-scale orbital effects. This results in rather stable residual accelerations, as shown in Figure 6, enabling this investigation of mass density–wind ambiguities surrounding the ETA.

Small changes in the relative acceleration were observed between the ascending and descending orbits for a given local time. If attributing these changes solely to wind, then using the sensitivity analysis in Figure 2 and the calculated average distance between the ascending and descending acceleration residual of 1.2% reveal that the average velocity difference would be about 50 m/s. A change in 50 m/s between the ascending and descending orbits corresponds to a 25 m/s meridional wind perturbation, which is on the order of magnitude of winds captured

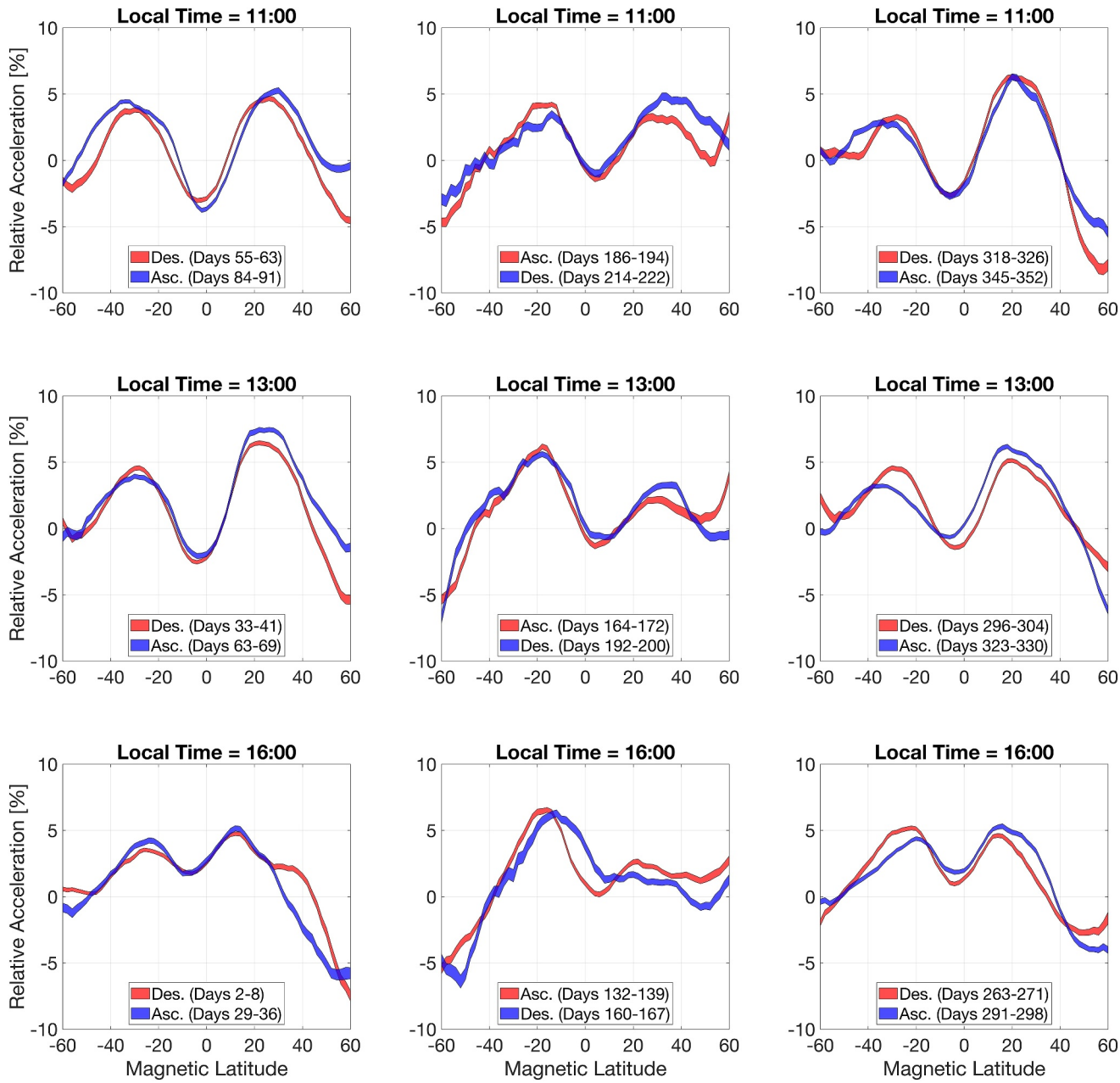

Figure 6. Relative acceleration (percent change) profiles with respect to magnetic latitude for ascending/descending orbits in 2003 (red) and 2004 (blue). Each column presents three local time profiles within a similar season and the widths of the lines quantify the uncertainty of the mean.

from past observations (e.g., Kawamura et al., 2000; Yamazaki et al., 2023). Taking this a step further, Figure 7 presents the extracted in-track wind perturbations with respect to magnetic latitude from the ADA technique after averaging wind estimates from all 30 min local time intervals between 9:00 and 16:00 LT for each seasonal period. The extracted wind perturbations show structure on the order of ±25 m/s with directions varying across the equatorial region from northward to southward. This assessment does not support the presence of large magnitude perturbations in meridional winds from 9:00 to 16:00 LT.

In addition to revealing that there are similarities in the ETA structure between 9:00–16:00 LT (and perhaps similar formation mechanisms), the ADA technique can also demonstrate local times where the equatorial behavior differs from the ETA structure. For example, when applying the ADA technique to data during 2003 and 2004 but at dusk local times, the results reveal distinctly different behavior from the 9:00 to 16:00 LT results.

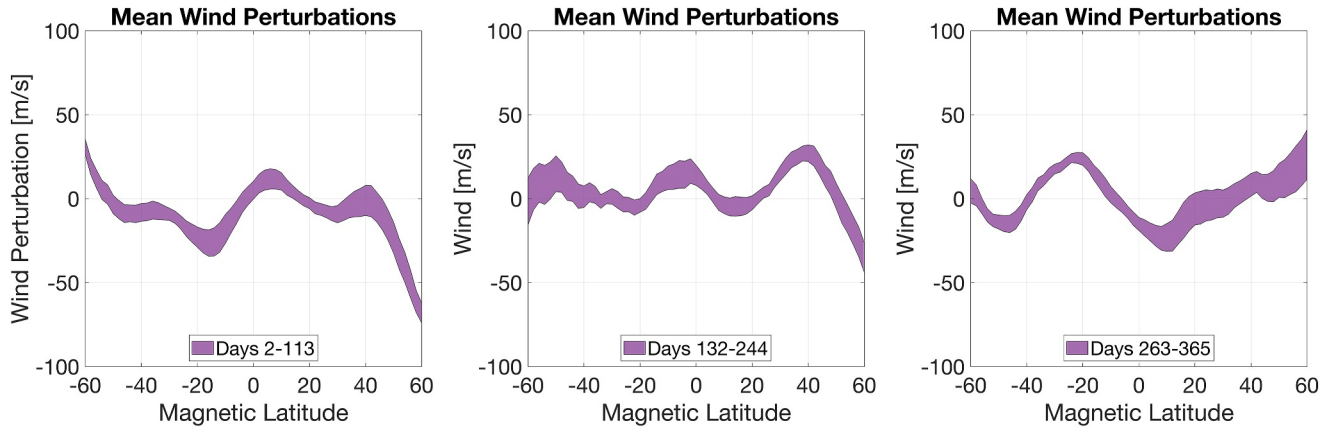

Figure 7. Mean in-track wind perturbation profiles from 9:00 to 16:00 LT with respect to magnetic latitude corresponding to the three seasons in Figure 6. The widths of the lines quantify the uncertainty of the mean.

Figure 8 shows the ascending and descending measurements at 18:00 LT where there appear to be opposing perturbations in acceleration. While this could be evidence of a wind-dominated feature per Section 2.2, it is important to revisit the ADA criteria in light of the multiple thermospheric processes that could be at play in the terminator region, such as those responsible for terminator waves (e.g., Forbes et al., 2008; Liu et al., 2009; Miyoshi et al., 2009). In the 9:00–16:00 LT section, the persistence criteria for the ETA is satisfied, with the main year-to-year difference observed is the magnitude of the ETA rather than a shift in its location. However, in the dusk sector Liu et al. (2009) observed a seasonal variation of the terminator waves due to the moving solar terminator, which can reverse the direction of the wavefronts between June and December solstice. This seasonal sensitivity could be why there is a shift in the peaks and valleys in Figure 8 considering the 28 day advancement between 2003 and 2004. This strong motion between seasons invalidates the ADA persistence criteria, making it challenging to definitively attribute any ascending/descending discrepancies to wind behavior. However, this behavior does support the hypothesis that the mechanisms ascribed to the ETA at 9:00–16:00 LT are distinct from those at play in the terminator region.

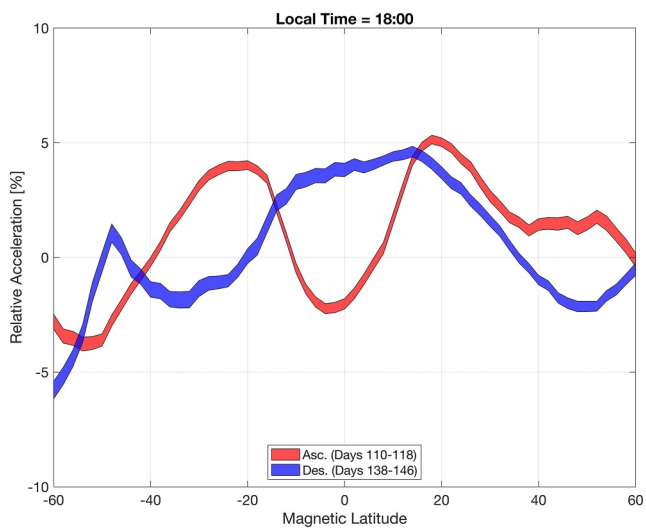

Figure 8. Relative acceleration (percent change) with respect to magnetic latitude for ascending/descending orbits in 2003 (red) and 2004 (blue) in the terminator region. The widths of the lines quantify the uncertainty of the mean.

5.2. ETA Formation

Using past satellite observations of the ionosphere and thermosphere, as well as ground-based observations, researchers have proposed several theories on the formation of the ETA and its coupling to the ionosphere. There have been studies ascribing zonal ion drag (Hedin & Mayr, 1973), meridional ion drag (Maruyama et al., 2003), field-aligned ion drag (Hsu et al., 2014; Lei et al., 2012), chemical heating (Fuller-Rowell et al., 1997), and circulation cell patterns (Clemmons et al., 2013; Miyoshi et al., 2011) to describe the observed behavior of various thermospheric properties associated with the ETA and ionosphere. From a holistic perspective, the formation mechanisms of the ETA remain inconclusive and involve several thermospheric properties, hence the multiple names and descriptions of the phenomenon that have emerged over the years. This can be attributed to some combination of varying instrument capabilities, sparse simultaneous observations of thermospheric and ionospheric properties, and differing interpretations of instrument measurements. In summary, past observations of the thermosphere and ionosphere suggest that the mechanisms behind the formation of the ETA have influences on the zonal wind, meridional wind, vertical wind, neutral temperature, neutral mass density, neutral composition, and various ionospheric properties spanning roughly 275–600 km in altitude and 11:00–21:00 LT. It is unlikely that the same processes are responsible for the dayside, duskside, and nightside structures as there are large differences in the ionospheric and thermospheric

composition, plasma density, wind behavior, neutral temperature, and neutral mass density.

A unifying theory would not only require simultaneous measurements of various thermospheric and ionospheric properties, but also require that the interpretation of the measurements have the capability to reveal similar mechanisms in the target region. The ADA technique has demonstrated that between 9:00 and 16:00 LT around 400 km, there are probably similar mechanisms occurring in the region considering that the acceleration perturbations behave similarly. Although the in-track wind perturbation magnitudes were determined insufficient to produce the majority of the observed acceleration perturbation structure surrounding the ETA, this conclusion does not suggest that a wind structure is not involved in the formation of the ETA. The work of Hsu et al. (2014) has shown by simulation that a weak divergence in the meridional wind caused by field-aligned ion drag is sufficient to induce vertical winds that cool the thermosphere and consequently produce a mass density trough over the magnetic equator of similar magnitude to observations. The derived wind structure in Figure 7 is suggestive of ETA formation mechanisms in the 9:00–16:00 LT, where divergent motion at the magnetic equator induces upward vertical winds that cool the region causing a trough in mass density and temperature at 400 km altitude. Observations outside of this local time range are not likely to be caused by the same process, which disputes past findings ascribing the ETA to dusk local times. The ADA technique has also confirmed that the ETA is persistent across all seasons, which means that resolving the ETA is not dependent on what time of year the measurements were taken.

6. Conclusion

The equatorial thermosphere anomaly (ETA) has been investigated, using accelerometer measurements from the CHAMP satellite at different orbital phases, to determine whether the feature is density-dominated, wind-dominated, or some combination of the two. The in-track ambiguity in mass density and wind associated with the observed ETA feature in the accelerometry data can be disentangled by taking advantage of the influence of the directionality of in-track winds on relative acceleration, while also emphasizing the potential differences when observing ascending and descending orbit data. The in-track acceleration perturbations surrounding the ETA were explored by introducing the ascending-descending accelerometer (ADA) technique as another means of analysis from drag accelerometry data. The ADA technique revealed that the ETA is a density-dominated feature between 9:00 and 16:00 LT near 400 km altitude from 2003 to 2004. This result indicates that changes in the acceleration due to wind can be considered small compared to the changes due to mass density in the equatorial region. It also suggests that the formation mechanism that creates the mass density feature across 9:00–16:00 LT are similar. The results differ for regions around the dusk terminator, but whether this is due to a persistent wind perturbation or simply a violation of the persistence of the underlying feature is difficult to resolve with the measurements available. Past analyses of the ETA utilize data between 11:00 and 21:00 LT in attempts to describe the ETA formation mechanisms, but the results suggest that outside of 9:00–16:00 LT, there might be a different cause, or perhaps, multiple mechanisms at play. This offers new insight as to the ETA formation mechanisms operating at specific local times. The results also reinforce past observations of the ETA that suggested a mass density feature that is persistent throughout all seasons.

With the growing abundance of accelerometry measurements and increasing instrument capabilities, there are several ways to expand this work to other regions of the thermosphere. The technique can be used to revisit the assumptions made on the in-track wind component from past mass density and cross-track wind derivations for missions that meet the ADA criteria, because it has been demonstrated that in-track winds cannot always be neglected. For the CHAMP mission, this technique can be applied to the entirety of the accelerometer data available from 2000 to 2010. For other satellites that carry multi-axis accelerometers at high inclination, such as GRACE, GRACE-FO, and the Swarm satellites, this technique can be used to analyze thermospheric perturbations a year apart or analyze the equinoxes within the same year. To add another level of complexity, the technique can be applied to several missions simultaneously or to multi-satellite constellation missions. For a constellation ADA analysis, one can either observe multiple local times at once, or even capture instances when satellites ascend and descend the same region simultaneously providing more temporal information on thermospheric structures. The ADA technique could also be applied to regions of interest where thermospheric density or wind processes are not fully understood, such as the terminator, high-latitude, and nightside regions. Under the right conditions, capturing simultaneous ascending and descending orbits of the same region can go beyond classifying a region as a density- or wind-dominated perturbation, but can more quantitatively extract the density and winds along those orbit paths.

Data Availability Statement

The acceleration data from CHAMP's STAR accelerometer used in this study is based on Sutton (2009) and can be downloaded from https://doi.org/10.5281/zenodo.10582349.

Acknowledgments
This work is based upon work supported by the National Science Foundation Graduate Research Fellowship under Grant DGE 2040434, the National Science Foundation Collaborative Research: CubeSat Ideas Lab: Space Weather Atmospheric Reconfigurable Multiscale Experiment (SWARM-EX) CubeSats under Award No. 1936665, the NASA GDC IDS under Contract No. 80GSFC22CA012, and the NASA Heliophysics Division Space Weather Science Application Initiative under Grant 80NSSC21K1554.

References

Bruinsma, S., & Biancale, R. (2003). Total densities derived from accelerometer data. *Journal of Spacecraft and Rockets*, *40*(2), 230–236. https://doi.org/10.2514/2.3937

Bruinsma, S., Siemes, C., Emmert, J. T., & Mlynczak, M. G. (2022). Description and comparison of 21st century thermosphere data. *Advances in Space Research*, *72*(12), 5476–5489. https://doi.org/10.1016/j.asr.2022.09.038

Clemmons, J. H., Walterscheid, R. L., Christensen, A. B., & Bishop, R. L. (2013). Rapid, highly structured meridional winds and their modulation by non migrating tides: Measurements from the Streak mission. *Journal of Geophysical Research: Space Physics*, *118*(2), 866–877. https://doi.org/10.1029/2012JA017661

Dhadly, M., Sassi, F., Emmert, J., Drob, D., Conde, M., Wu, Q., et al. (2023). Neutral winds from mesosphere to thermosphere—Past, present, and future outlook. *Frontiers in Astronomy and Space Sciences*, *9*, 1050586. https://doi.org/10.3389/fspas.2022.1050586

Doornbos, E. N., van den Ijssel, J., Luhr, H., Foerster, M., & Koppenwallner, G. (2010). Neutral density and crosswind determination from arbitrarily oriented multiaxis accelerometers on satellites. *Journal of Spacecraft and Rockets*, *47*(4), 580–589. https://doi.org/10.2514/1.48114

Drob, D. P., Emmert, J. T., Meriwether, J. W., Makela, J. J., Doornbos, E., Conde, M., et al. (2015). An update to the horizontal wind model (HWM): The quiet time thermosphere. *Earth and Space Science*, *2*(7), 301–319. https://doi.org/10.1002/2014EA000089

Emmert, J. T., Drob, D. P., Picone, J. M., Siskind, D. E., Jones, M., Mlynczak, M. G., et al. (2020). Nrlmsis 2.0: A whole atmosphere empirical model of temperature and neutral species densities. *Earth and Space Science*, *7*(3), e2020EA001321. https://doi.org/10.1029/2020EA001321

Floberghagen, R., Fehringer, M., Lamarre, D., Muzi, D., Frommknecht, B., Steiger, C., et al. (2011). Erratum to: Mission design, operation and exploitation of the Gravity field and steady-state Ocean Circulation Explorer (GOCE) mission. *Journal of Geodesy*, *85*(11), 749–758. https://doi.org/10.1007/s00190-011-0498-3

Forbes, J. M., Bruinsma, S. L., Miyoshi, Y., & Fujiwara, H. (2008). A solar terminator wave in thermosphere neutral densities measured by the CHAMP satellite. *Geophysical Research Letters*, *35*(14), L14802. https://doi.org/10.1029/2008GL034075

Fuller-Rowell, T. J., Codrescu, M. V., Fejer, B. G., Borer, W., Marcos, F., & Anderson, D. N. (1997). Dynamics of the low-latitude thermosphere: Quiet and disturbed conditions. *Journal of Atmospheric and Terrestrial Physics*, *59*(13), 1533–1540. https://doi.org/10.1016/S1364-6826(96)00154-X

Hedin, A. E., & Mayr, H. G. (1973). Magnetic control of the near equatorial neutral temperature. *Journal of Geophysical Research*, *78*(10), 1688–1691. https://doi.org/10.1029/ja078i010p01688

Hsu, V. W., Thayer, J. P., Lei, J., & Wang, W. (2014). Formation of the equatorial thermosphere anomaly trough: Local time and solar cycle variations. *Journal of Geophysical Research: Space Physics*, *119*(12), 10456–10473. https://doi.org/10.1002/2014JA020416

Kawamura, S., Otsuka, Y., Zhang, S.-R., Fukao, S., & Oliver, W. L. (2000). A climatology of middle and upper atmosphere radar observations of thermospheric winds. *Journal of Geophysical Research*, *105*(A6), 12777–12788. https://doi.org/10.1029/2000JA900013

Kornfeld, R. P., Arnold, B. W., Gross, M. A., Dahya, N. T., Klipstein, W. M., Gath, P. F., & Bettadpur, S. (2019). GRACE-FO: The gravity recovery and climate experiment follow-on mission. *Journal of Spacecraft and Rockets*, *56*(3), 931–951. https://doi.org/10.2514/1.A34326

Lei, J., Burns, A. G., Thayer, J. P., Wang, W., Mlynczak, M. G., Hunt, L. A., et al. (2012). Overcooling in the upper thermosphere during the recovery phase of the 2003 October storms. *Journal of Geophysical Research*, *117*(A3), A03314. https://doi.org/10.1029/2011JA016994

Lei, J., Thayer, J. P., & Forbes, J. M. (2010). Longitudinal and geomagnetic activity modulation of the equatorial thermosphere anomaly. *Journal of Geophysical Research*, *115*(A8), A08311. https://doi.org/10.1029/2009JA015177

Liu, H., Lühr, H., Henize, V., & Köhler, W. (2005). Global distribution of the thermospheric total mass density derived from CHAMP. *Journal of Geophysical Research*, *110*(A4), A04301. https://doi.org/10.1029/2004JA010741

Liu, H., Lühr, H., & Watanabe, S. (2007). Climatology of the equatorial thermospheric mass density anomaly. *Journal of Geophysical Research*, *112*(A5), A05305. https://doi.org/10.1029/2006JA012199

Liu, H., Lühr, H., & Watanabe, S. (2009). A solar terminator wave in thermospheric wind and density simultaneously observed by champ. *Geophysical Research Letters*, *36*(10), L10109. https://doi.org/10.1029/2009gl038165

Liu, H., Lühr, H., Watanabe, S., Köhler, W., Henize, V., & Visser, P. (2006). Zonal winds in the equatorial upper thermosphere: Decomposing the solar flux, geomagnetic activity, and seasonal dependencies. *Journal of Geophysical Research*, *111*(A7), A07307. https://doi.org/10.1029/2005JA011415

Lühr, H., Rentz, S., Ritter, P., Liu, H., & Häusler, K. (2007). Average thermospheric wind patterns over the polar regions, as observed by CHAMP. *Annals of Geophysics*, *25*(5), 1093–1101. https://doi.org/10.5194/angeo-25-1093-2007

Maruyama, N., Watanabe, S., & Fuller-Rowell, T. J. (2003). Dynamic and energetic coupling in the equatorial ionosphere and thermosphere. *Journal of Geophysical Research*, *108*(A11), 1396. https://doi.org/10.1029/2002JA009599

Miyoshi, Y., Fujiwara, H., Forbes, J. M., & Bruinsma, S. L. (2009). Solar terminator wave and its relation to the atmospheric tide. *Journal of Geophysical Research*, *114*(A7), A07303. https://doi.org/10.1029/2009JA014110

Miyoshi, Y., Fujiwara, H., Jin, H., Shinagawa, H., Liu, H., & Terada, K. (2011). Model study on the formation of the equatorial mass density anomaly in the thermosphere. *Journal of Geophysical Research*, *116*(A5), A05322. https://doi.org/10.1029/2010JA016315

Olsen, N., Friis-Christensen, E., Floberghagen, R., Alken, P., Beggan, C. D., Chulliat, A., et al. (2013). The Swarm satellite constellation application and Research facility (SCARF) and Swarm data products. *Earth Planets and Space*, *65*(11), 1189–1200. https://doi.org/10.5047/eps.2013.07.001

Philbrick, C. R., & McIsaac, J. P. (1972). Measurements of atmospheric composition near 400 km. *Space Research*, *12*, 743–750.

Picone, J. M., Hedin, A. E., Drob, D. P., & Aikin, A. C. (2002). NRLMSISE-00 empirical model of the atmosphere: Statistical comparisons and scientific issues. *Journal of Geophysical Research*, *107*(A12), 1468. https://doi.org/10.1029/2002JA009430

Qian, L., Burns, A. G., Emery, B. A., Foster, B., Lu, G., Maute, A., et al. (2014). The ncar TIE-GCM: A community model of the coupled thermosphere/ionosphere system. In J. Huba, R. Schunk, & G. Khazanov (Eds.), *Modeling the ionosphere-thermosphere system*, AGU Geophysical Monograph Series (pp. 73–83). https://doi.org/10.1002/9781118704417.ch7

Raghavarao, R., Hoegy, W. R., Spencer, N. W., & Wharton, L. E. (1993). Neutral temperature anomaly in the equatorial thermosphere – a source of vertical winds. *Geophysical Research Letters*, *20*(11), 1023–1026. https://doi.org/10.1029/93GL01253

Raghavarao, R., Wharton, L. E., Spencer, N. W., Mayr, H. G., & Brace, L. H. (1991). An equatorial temperature and wind anomaly (ETWA). *Geophysical Research Letters*, *18*(7), 1193–1196. https://doi.org/10.1029/91GL01561

Reigber, C., Lühr, H., & Schwintzer, P. (2002). CHAMP mission status. *Advances in Space Research*, *30*(2), 129–134. https://doi.org/10.1016/s0273-1177(02)00276-4

Reigber, C., Lühr, H., & Schwintzer, P. (Eds.). (2003). *First CHAMP mission results for gravity, magnetic and atmospheric studies* (pp. 129–134). Springer Berlin Heidelberg. https://doi.org/10.1007/978-3-540-38366-6

Richmond, A. D. (1983). Thermospheric dynamics and electrodynamics. In R. L. Carovillano & J. M. Forbes (Eds.), *Solar-terrestrial Physics* (pp. 523–607). D. Reidel.

Siemes, C., Borries, C., Bruinsma, S., Fernandez-Gomez, I., Hładczuk, N., den Ijssel, J., et al. (2023). New thermosphere neutral mass density and crosswind datasets from CHAMP, GRACE, and GRACE-FO. *Journal of Space Weather and Space Climate*, *13*, 16. https://doi.org/10.1051/swsc/2023014

Sutton, E. K. (2009). Normalized force coefficients for satellites with elongated shapes. (Vol. *46*, pp. 112–116). https://doi.org/10.2514/1.40940. [Dataset] Version 2.3. *Journal of Spacecraft and Rockets1*.

Sutton, E. K., Forbes, J. M., & Nerem, R. S. (2005). Global thermospheric neutral density and wind response to the severe 2003 geomagnetic storms from CHAMP accelerometer data. *Journal of Geophysical Research*, *110*(A9), A09S40. https://doi.org/10.1029/2004JA010985

Sutton, E. K., Nerem, R. S., & Forbes, J. M. (2007). Density and winds in the thermosphere deduced from accelerometer data. *Journal of Spacecraft and Rockets*, *44*(6), 1210–1219. https://doi.org/10.2514/1.28641

Tapley, B. D., Bettadpur, S., Watkins, M., & Reigber, C. (2004). The gravity recovery and climate experiment: Mission overview and early results. *Geophysical Research Letters*, *31*(9), 9607. https://doi.org/10.1029/2004GL019920

Thayer, J. P., Lei, J., Forbes, J. M., Sutton, E. K., & Nerem, R. S. (2008). Thermospheric density oscillations due to periodic solar wind high-speed streams. *Journal of Geophysical Research*, *113*(A6), A06307. https://doi.org/10.1029/2008JA013190

Yamazaki, Y., Harding, B. J., Qiu, L., Stolle, C., Siddiqui, T. A., Miyoshi, Y., et al. (2023). Monthly climatologies of zonal-mean and tidal winds in the thermosphere as observed by ICON/MIGHTI during April 2020–March 2022. *Earth and Space Science*, *10*(6), e2023EA002962. https://doi.org/10.1029/2023EA002962